biophysica

MDPI

Article

A Vision-Based Photoanthropometric Approach for Yoga Pose Analysis Using LabVIEW-ML

T. P. Kausalya Nandan * and S. Saradha Rani

Department of Electrical, Electronics and Communication Engineering, GITAM School of Technology, GITAM (Deemed to be University), Visakhapatnam 530045, Andhra Pradesh, India; ssabbava@gitam.edu
* Correspondence: srinivaskausalyanandan@gmail.com or 121960404014@gitam.in

Abstract

In this work, we present a novel framework of integrating anthropometric measurement with posture recognition using LabVIEW's Vision Development Module specifically for yoga poses. Yoga is a practice that originated in India many years ago and is now popular globally, contributing significantly towards balancing the human body and mind. A key challenge is the accurate recognition of yoga poses in real time using contactless techniques. To achieve this, the proposed system works by digitizing yoga poses through anthropometric measurements enhanced through photoanthropometric modeling with Calibrated Bounding Boxes using YOLO version 4 for representing the poses, combined with geometric examinations to normalize bounding box dimensions and proceed for pose variations. The intermediate model developed improves the measurement accuracy, while the final stage handles posture classification in the LabVIEW ML environment for real-time yoga pose recognition. This study focuses on the Tadasana pose. A Microsoft XBOX 360 Kinect sensor was used for capturing the images, which were processed using LabVIEW 2019 Vision IMAQ. An inference model was developed for feature extraction and matching, such that precise posture identification was facilitated with bounding boxes. The experimental results illustrate that the proposed system achieves a pose recognition accuracy, with respect to anthropometric measurements, of 95.4%, thus proving its potential for rehabilitation and health monitoring.

Keywords: anthropometric measurements; yoga posture; tadasanas; LabVIEW Vision

1. Introduction

Yoga helps to prevent non-communicable diseases (NCDs) while promoting both physical and mental health, as validated by the World Health Organization (WHO). NCDs account for over 80% of premature deaths, 85% of which occur in low- and middle-income countries. Yoga decreases the heart rate, controls anxiety and stress, and improves psychological well-being, making it a beneficial practice for individuals suffering from illnesses, unlike other physical activities. The WHO Global Centre for Traditional Medicine (a USD 250 million investment) suggested that yoga should be regarded as a main approach for achieving both universal health and the Sustainable Development Goal (SDG) of reducing physical inactivity by 15% by 2030 [1] globally.

Regularly practicing yoga significantly improves an individual's psychological well-being by enhancing their vitality, focus, endurance, resilience, and inner tranquility [2]. With advancements in computer vision and image processing techniques, yoga pose recognition has been investigated and thus the knowledge on yoga poses for real-time technological

Check for updates

Academic Editor: Matthias Buck

Received: 31 May 2026
Revised: 11 July 2026
Accepted: 13 July 2026
Published: 20 July 2026

 https://doi.org/10.3390/biophysica6040064

applications has been enhanced. M. Sathyanarayanan et al. [3] emphasized in their work on vision-based recognition that performance depended on the type of camera used across a wide range of computer vision tasks, ranging from fundamental operations such as feature detection, motion estimation, and optical flow analysis to major processes including 3D reconstruction, image segmentation, and object recognition [4,5].

In this context, pose-based recognition methods are widespread. Human action recognition studies have been conducted (for example, by S. Zhang et al. [6]), with convolutional neural networks (CNNs) and artificial neural networks (ANNs) being the most commonly used approaches for pose estimation. Wei et al. [7] proposed graph-based convolutional networks for yoga pose recognition, and histogram models have also been used for pose detection in humans [8]. Human movement and activity are often recognized using skeleton-based approaches. A. Raza et al. [9] investigated physiotherapy exercises by analyzing skeletal features and applying the Logistic Regression Recursive Feature Elimination (LogRF) method for optimization. However, skeletal models are often limited at the fine limb edges and in motion tracking. In contrast, computer vision-based methods have demonstrated better accuracy. The Speeded-Up Robust Features (SURF) algorithm, which has been a popular choice for over a decade, has been effective in detecting human motion [10]. V. Bhandage et al. [11] estimated yoga Surya Namaskar poses using CNN, HOG, and SURF.

One of the major bottlenecks in human pose estimation lies in correlating the real-world height of an individual with computer vision-based techniques. Distance-based measurements have had an appreciable impact in estimating height, in which anthropometric measurements play a key role. One study [12] provides an elaborated discussion of measurement frameworks adopted by various organizations, including mesh models, 3D scanning, and image feature-based methods. N. Sarafianos et al. [13] computed the height of a human considering anthropometric ratios and support vector regression, while the latest implementations have combined anthropometric principles with deep learning frameworks for improved human size and height estimation [14]. David A. Winter [15] conducted experimental studies on height-based estimations of human body dimensions, significantly contributing to anthropometric research. This study has also acted as the basis for modeling biomechanical patterns in athletes. Height estimation using marker less, deep-learning-based approaches has been reported in [16,17].

The proposed method introduces a unique framework that employs anthropometric measurements to estimate yoga poses:

1. The proposed method employs a novel design that evaluates an individual subject's height and body proportions using digitized anthropometric measurements while the yoga poses are performed.
2. The system uses standardized anthropometric parameters which ensure accurate and efficient computational analysis for angle-oriented human body posture alignment.
3. The proposed system integrates the YOLO model with photometric anthropometry using vision-based techniques for bounding boxes, which enables the precise detection and measurement of various human features in yoga poses.

YOLOv4 provides fast and reliable human body identification; however, it does not directly estimate the anatomical body proportions required for accurate yoga pose evaluation. To overcome this limitation, the proposed method integrates YOLOv4-based detection with photoanthropometric modeling, in which body segment dimensions are estimated using established anthropometric relationships. These measurements enable the assessment of limb proportions, body alignment, and posture geometry while avoiding the computational complexity associated with conventional skeleton-based pose estimation methods. The resulting framework is computationally efficient, interpretable, and well suited for real-time yoga pose analysis.

This section gives an overview of the basic requirements and foundations for anthropometric measurements. This background analysis laid a foundation for the development of a photoanthropometric analysis for yoga pose assessment, as detailed in Section 2. Section 3 deals with the embedded architecture for photoanthropometric analysis. Section 4 highlights the experimental validation and provides a discussion of the proposed work. Finally, Section 5 concludes the work and proposes future research directions.

2. Methodology

This study focuses on photoanthropometric measurements of humans in yoga poses analyzed using a computer vision-based LabVIEW machine learning framework.

2.1. Anthropometric Measurement of Human Posture

The proposed method is integrated in line with the standard practices developed by David A Winter [15] for anthropometric measurements, where body segment lengths are expressed as shown in Figure 1. Human height (H) serves as the standard reference for computing the remaining parts of the human body. In practice, bounding boxes are utilized for such computations; however, achieving an adequate measurement accuracy remains a bottleneck challenge. In this regard, the present work addresses this challenge by employing computer vision techniques integrated with anthropometric measurements.

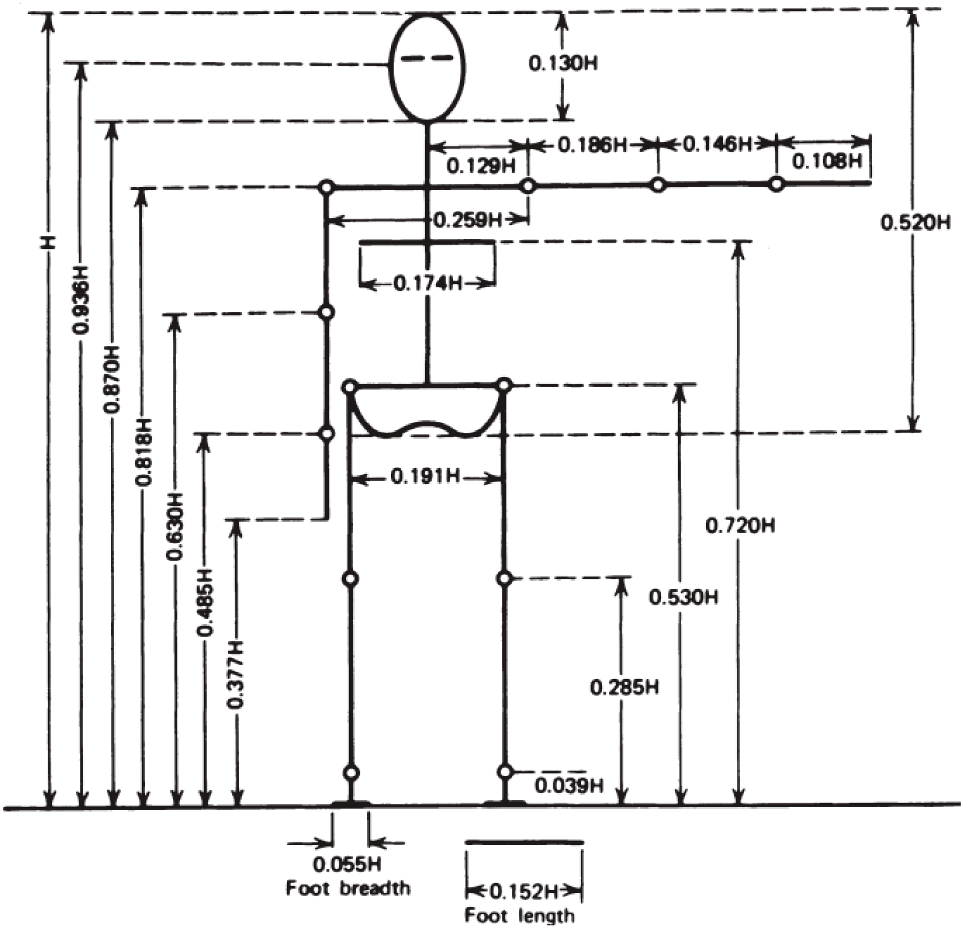

Figure 1. Anthropometric measurements for body segment lengths [15].

The size of the human head (L_{head}) is captured using a bounding box, which serves as the reference point for estimating the size of the remaining parts of the human body. The five major human metrics are the head-to-height ratio, upper limb length, lower limb length, torso height and reach height.

a. Head-to-height ratio:

$$L_{head} = K_{hhead} H \tag{1}$$

$$H = \frac{L_{hhead}}{K_{hhead}} \tag{2}$$

Equations (1) and (2) define the final bounding box height as the head height (L_{head}). The total human height (H) is then computed using the standard proportional constant $K_{hhead} = 0.130$, as reported by Winter [15].

b. Upper limb length:

$$L_{upper\_limb} = \frac{K_{upper\_limb}}{K_{head}} L_{head} \tag{3}$$

$$\boldsymbol{L_{upper\_limb} \propto L_{hhead}} \tag{4}$$

$$K_{upper\_limb} = (\ Shoulder - elbow) + (Elbow - wrist) + (Wrist - fingertip) \tag{5}$$

The proportional constant K_{upper_limb} comprises three components of the arm—upper arm, forearm, and hand—and has a standard value of 0.440, as presented in Equation (5). The relationship established between the upper limb and the head corresponds to a ratio of 3.38, as shown in Equation (3). The head height is always directly proportional to the upper limb length, as expressed in Equation (4).

Similarly, the length of the human body is measured using the following expressions for the lower limb, torso height, and reach height:

$$\boldsymbol{L_{lower\_limb} = \frac{K_{lower\_limb}}{K_{hhead}} L_{hhead}} \tag{6}$$

According to the above expressions, each body segment is proportionally related to the head height. The total body height is estimated from the head, and other segmental dimensions are derived using standard anthropometric ratios. This proportional approach enables accurate body part size estimation using only the bounding box of the head. This approach represents a novel method for estimating human postures.

c. Computation of posture angle deviation using landmark vectors

The posture angle deviation can take two forms: (i) deviation with respect to front/back or right/left bending, and (ii) deviation in human height caused by stretching of the lower limbs.

i. Directional Posture Deviation

$$\text{The hip is the pivot: } P = (x_h, y_h) \tag{7}$$

The top of the head has coordinates in two different postures:

$$T_1 = (x_{t1}, y_{t1}) \text{ and } T_2 = (x_{t2}, y_{t2}) \tag{8}$$

Vectors are computed as a and b.

$$a = \overrightarrow{PT1} = (\mathrm{x_{t1}} - \mathrm{x_h},\ \mathrm{y_{t1}} - \mathrm{y_h}) \tag{9}$$

$$b = \overrightarrow{PT2} = (\mathrm{x_{t2}} - \mathrm{x_h},\ \mathrm{y_{t2}} - \mathrm{y_h}) \tag{10}$$

Compute absolute orientation of head–hip line in each pose is calculated as

$$\alpha = atan2(\mathrm{yt1} - \mathrm{yh}, \mathrm{xt1} - \mathrm{xh}) \tag{11}$$

$$\beta = btan2(\mathrm{yt2} - \mathrm{yh}, \mathrm{xt2} - \mathrm{xh}) \tag{12}$$

Posture deviation from origin to other side:

$$\Delta\theta raw = |\beta - \ \alpha| \tag{13}$$

Wrap to the principal range 0–180°:

$$\Delta\theta = \min(\Delta\theta raw,\ 360 - \Delta\theta raw) \tag{14}$$

ii. Vertical Posture Deviation

Human posture height deviation is computed using the vertical posture deviation:

$$\Delta H = H - H1 \tag{15}$$

Length of the lower limb ($\mathrm{L_{limb}}$) is generically defined (Figure 2).

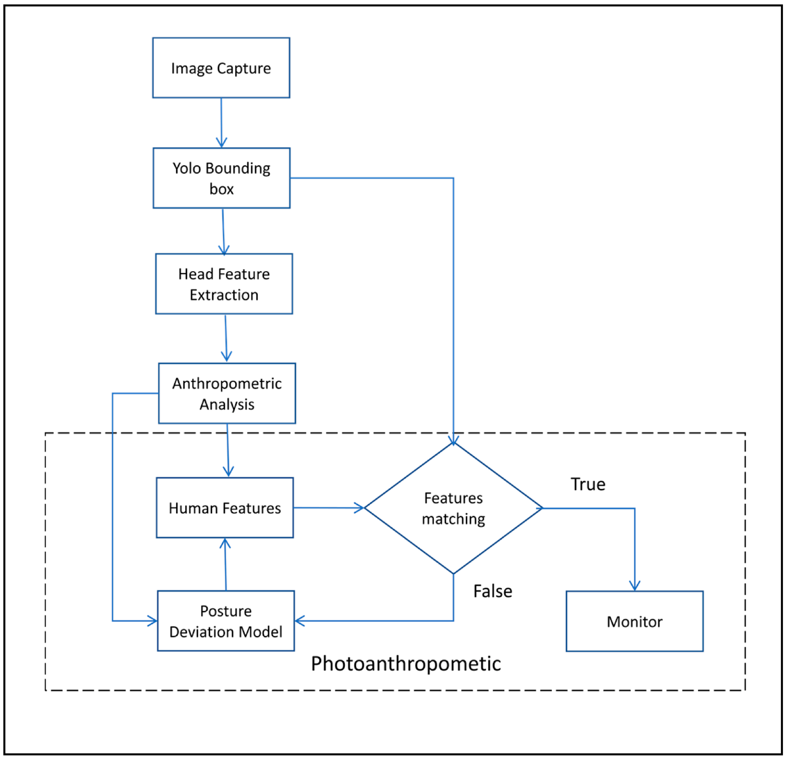

Figure 2. Flowchart for human posture analysis.

$\mathrm{L_{limb}}$ = 0.53H, which is the angle of deviation by stretching of the lower limbs:

$$\theta_{\mathrm{limbs}} = \mathrm{Sin}^{-1}(\Delta \boldsymbol{H}/\mathrm{L_{limb}}) \tag{16}$$

https://doi.org/10.3390/biophysica6040064

2.2. Posture Analysis Using Photoanthropometric

Human posture is analyzed taking a photoanthropometric approach, as illustrated in Figure 2. The proposed method avoids the need for training datasets by relying on anthropometric measurements. In this study, a pre-trained YOLOv4 model for human body localization is employed and therefore does not require additional task-specific training or retraining for yoga pose analysis. Once the body region is detected, posture is evaluated using photoanthropometric measurements derived from established anthropometric relationships rather than learning-based pose estimation. Consequently, the proposed method eliminates the need to collect and annotate a dedicated yoga pose dataset or retrain the detection model, thereby reducing computational complexity and development demands while maintaining reliable real-time performance.

In this process, a Kinect camera was used to capture images of a subject performing various yoga poses. These images are processed using a single-stage detector, YOLOv4, for human detection and classification. In the post-processing stage of YOLOv4, a generic Non-Maximum Suppression (NMS) algorithm is applied to identify the subject with the highest confidence score. From the detected subject, head-related features are extracted and estimated as L_{head}, which serves as an input for the anthropometric measurement module.

In the analysis of yoga poses, photoanthropometric measurements play a vital role. Five standard anthropometric features of the human body are compared during the feature-matching stage. Successful feature matching confirms that the intended pose has been correctly performed. If the extracted features do not match the expected anthropometric pattern of the pose, the deviation is estimated. The system then computes the anthropometric measurements corresponding to this deviation, enabling precise quantification of pose differences.

3. Vision-Based Embedded System for Real-Time Human Posture Analysis

Figure 3 presents the design of the system for estimating human poses through computer vision-based photoanthropometric analysis. The architecture (as shown in Figure 3) captures human yoga poses using a camera and processes them through a computer vision-based YOLOv4 model integrated with convolution layers for feature extraction and fully connected (FC) layers for classification and bounding box generation. The bounding boxes serve as the primary input for analyzing the human postures using a posture analysis module. The integrated posture analysis module represents a novel contribution in the form of a photoanthropometric model that employs runtime inference approaches.

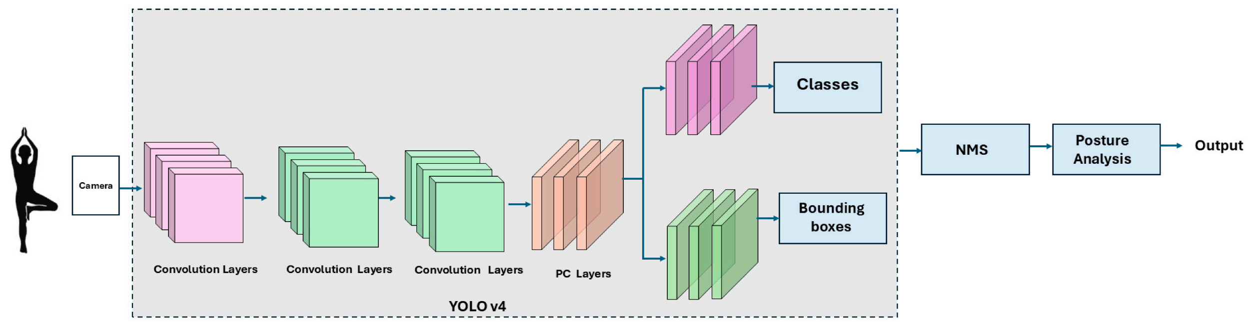

Figure 3. Overall system architecture for human yoga pose estimation using photoanthropometry.

3.1. Embedded Architectures for Posture Analysis

The embedded posture analysis architecture constitutes the post-processing stage of the proposed yoga pose estimation framework and operates based on the results generated by the YOLOv4 pipeline, as shown in Figure 3. After object detection, the Non-Maximum Suppression (NMS) module filters out any overlap using a confidence threshold of 0.5 and selects the most reliable human head bounding box. The refined head region subsequently enters the embedded posture analysis architecture for anthropometric measurement and posture evaluation.

The architecture comprises five software modules, as shown in Figure 4: feature extraction, anthropometric measurement, photoanthropometric analysis, soft-control unit, and monitoring module. The soft-control unit acts as the central controller, coordinating the execution of all processing stages through an event-driven mechanism and a bidirectional control bus. This synchronization ensures that each module executes sequentially while maintaining reliable data transfer throughout the embedded processing pipeline.

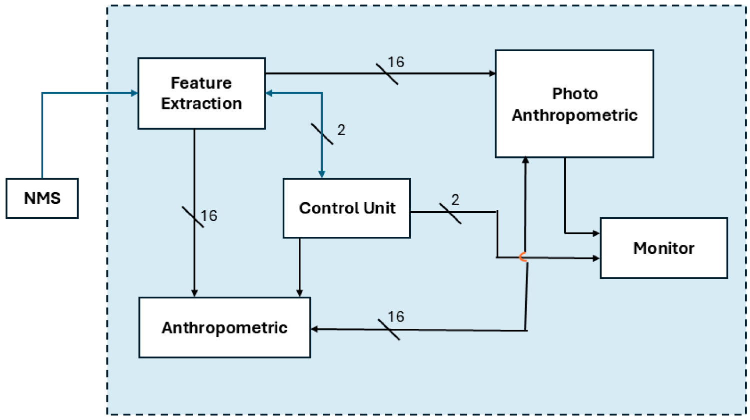

Figure 4. Embedded posture analysis architecture.

The Feature Extraction module receives the head bounding box generated after NMS and computes the head length by utilizing the bounding box coordinates. To improve localization accuracy, an internal Intersection-over-Union (IoU) is computed before the head dimensions are finalized. This feature extraction strategy represents a key contribution of the proposed work, as it enables a robust estimation of anthropometric parameters directly from the detected region without requiring additional sensing hardware.

The extracted head measurements are then supplied to the anthropometric measurement module, where body segment dimensions are estimated using established photoanthropometric relationships. Based on the measured head length, proportional dimensions of other body segments are calculated according to the standard anthropometric methodology described in [15]. These estimated body measurements provide the geometric foundation for posture evaluation.

Subsequently, the computed anthropometric measurements are processed by the photoanthropometric analysis module, which derives posture-related geometric features, including body alignment, limb proportions, joint orientation, and posture angles. These features are evaluated against the predefined geometric constraints of individual yoga poses to determine the correctness of the performed pose.

Finally, the recognized yoga pose together with the estimated anthropometric measurements are displayed through the monitoring module implemented in the LabVIEW graphical user interface, providing real-time visual feedback to the user. The numerical annotations shown along the communication paths in the architecture represent the bit widths of the data transferred between software modules, where 16-bit data buses are employed for anthropometric and feature information, while 2-bit control signals are used for synchronization and module coordination. This lightweight embedded architecture enables efficient real-time posture analysis while maintaining a low computational overhead and reliable execution within the LabVIEW environment.

3.2. Internal Architecture of Anthropometric Measurements

The internal architecture of the proposed anthropometric measurement module is illustrated in Figure 5. This module receives the refined head bounding box generated by the NMS stage of the object detection pipeline and converts it into anthropometric measurements required for yoga pose evaluation. The architecture consists of five functional stages: Feature Selection, Head Feature estimation, anthropometric computation, encoder, and output interface. The numerical annotations shown on the communication paths indicate the bit widths of the data transferred between processing blocks, where 3-bit signals represent the anthropometric feature selection coefficients, while 16-bit signals correspond to the computed measurement values exchanged between arithmetic modules.

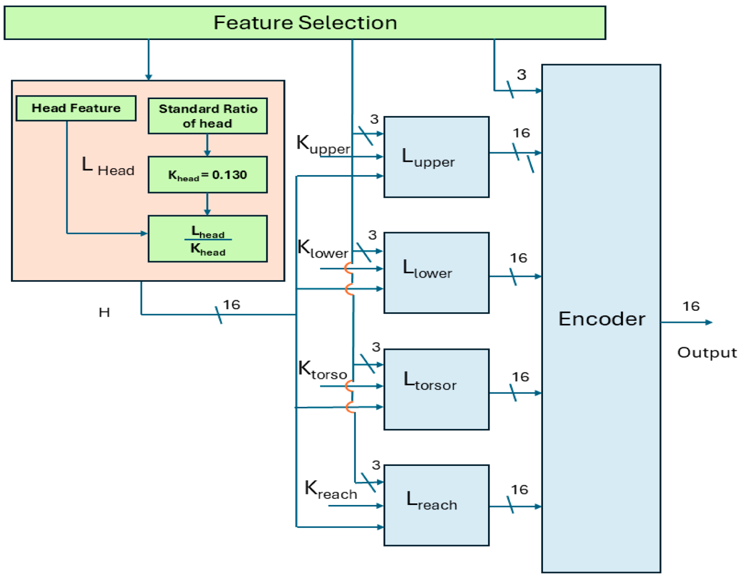

Figure 5. Internal architecture of anthropometric features.

The processing begins with the Feature Selection block, which controls the computation of the required anthropometric parameters according to the posture analysis stage. This block enables only the relevant measurement paths, thereby minimizing unnecessary computations and improving computational efficiency. The selected feature information is simultaneously forwarded to the corresponding anthropometric computation blocks and to the encoder through 3-bit control signals.

The Head Feature block receives the head bounding box extracted from the NMS output and determines the head length (L_{Head}) using the bounding box coordinates. Since the human head provides a stable anatomical reference, it serves as the primary measurement for estimating all remaining body dimensions. The standard anthropometric head-to-height ratio, K_{head} = 0.130, adopted from the photoanthropometric model reported in [15], is stored as a constant within this module. An arithmetic division operation computes $H = K_{head}/L_{head}$, where H represents the estimated total body height. The resulting body height is represented as a 16-bit value and distributed to all subsequent anthropometric computation modules.

Using the estimated body height, four dedicated computation blocks determine the principal body dimensions required for posture assessment. The Upper Limb Module calculates the upper body length (L_{upper}) using the proportional constant K_{upper}, while the Lower Limb Module estimates the lower body length (L_{lower}) using K_{lower}. Similarly, the Torso Module computes the torso height (L_{torso}) based on K_{torso}, and the Reach Module estimates the arm reach (L_{reach}) using the proportional constant K_{reach}. Each module performs an independent arithmetic operation using the common body height estimate and its corresponding anthropometric ratio, thereby allowing all body dimensions to be computed in parallel. The computed measurements are transferred as 16-bit outputs, ensuring sufficient numerical precision for subsequent posture analysis.

The computed anthropometric features are finally collected by the Encoder, which consolidates the measurements into a unified data stream for the posture evaluation module. In addition to aggregating the feature values, the encoder preserves the feature selection information received through the 3-bit control signals, ensuring that the posture analysis stage correctly interprets the transmitted anthropometric parameters. The encoder produces a 16-bit output that forms the input to the embedded posture analysis architecture described in the subsequent section.

Overall, the proposed architecture transforms a single head measurement extracted from the detected bounding box into multiple anthropometric body dimensions through proportional estimation. This modular design reduces computational complexity while providing a compact and hardware-friendly implementation suitable for real-time embedded yoga pose analysis.

3.3. Internal Photoanthropometric Architecture

The anthropometric feature vector is compared against the real-time image feature vector using Euclidean and weighted distance metrics within the feature-matching module. Frames exhibiting minimal distance are classified as valid posture accomplishments, whereas frames showing significant feature deviations are forwarded to the posture deviation analysis module, which is composed of four components, as shown in Figure 6: the feature-deviation unit, the vertical-deviation unit, the direction-deviation unit, and the hybrid deviation module. The feature-deviation unit determines the type of deviation and classifies it as either a vertical or directional deviation based on the observed feature differences.

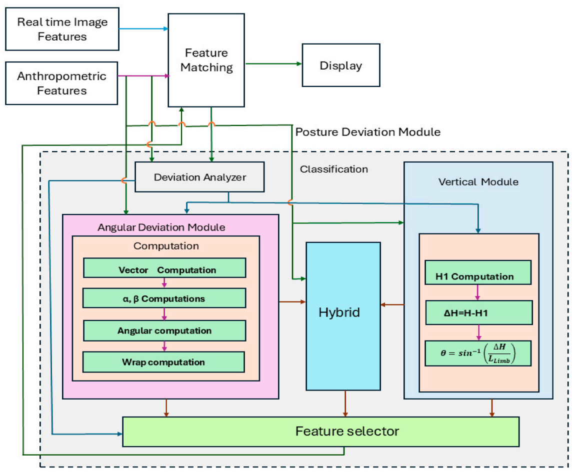

Figure 6. Internal photoanthropometric architecture.

The vertical deviation is computed when the human height changes from the original reference position, typically due to downward body movement. When the bounding box fails to capture the head region according to the actual image height, the resulting height difference is denoted as H1. This deviation corresponds to the stretch occurring in the lower limbs and is represented as ΔH. The height difference is further used to estimate the stretch length in the lower limbs and the angle formed between the hip and the lower limb segments. All these computations are derived using standard anthropometric measurement principles.

The angular-deviation unit generates posture vectors between the reference and observed frames and computes the associated orientation angles α and β. Their difference yields the angular deviation, which is subsequently quantized to a rounded angular value. A hybrid deviation module combines both vertical and angular deviation measures for composite analysis. A deviation-classification and feature selection mechanism determines the appropriate deviation category, selects the relevant deviation parameters, and forwards them through the encoder to the feature-matching stage.

4. Results of Embedded Yoga Poses

4.1. Experimental Setup of Yoga Studio

The proposed approach was validated using a dedicated experimental setup designed for yoga pose analysis, as shown in Figure 7. The setup consists of both hardware and software, along with the necessary logistical components. Visual data was captured using an Microsoft Xbox 360 Kinect RGB camera (resolution 1280 × 960 @ 12 fps), and an Intel® Core™ i5-8250U CPU laptop with configuration 12 Gb RAM, 512 GB SSD was used for processing. A green cloth backdrop was arranged to minimize background interference, and enable the computer vision model (YOLO + LabVIEW) to easily distinguish the person from the background. The Kinect sensor was positioned approximately 7 feet from the yoga mat. The software environment used for implementation was LabVIEW 2021, and the machine learning (ML)-based YOLOv4 Computer Vision VI module was integrated to validate the proposed methodology.

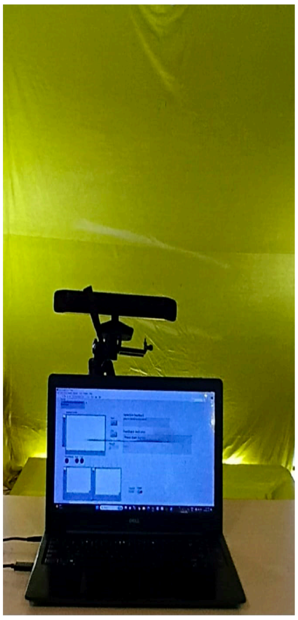

Figure 7. Experimental setup for yoga pose analysis.

4.2. Anthropometric Data Analysis

Figure 8 presents the performance of the proposed anthropometric computation framework, evaluated by comparing the subject's actual measurements with the corresponding theoretical anthropometric ratios (S1) for the values represented in Table 1. In the process of our implementation, the head height was first measured from the detected head region. Using this head measurement, the remaining body segment dimensions (upper limb, lower limb, torso, etc.) were estimated using standard anthropometric proportions. To quantify the variation between the two sets of values, the percentage deviation for each body segment was computed using the theoretical (T_i) and practical (P_i) measurements, based on the following percentage deviation formula:

$$\delta_i = (P_i - T_i)/T_i \times 100 \tag{17}$$

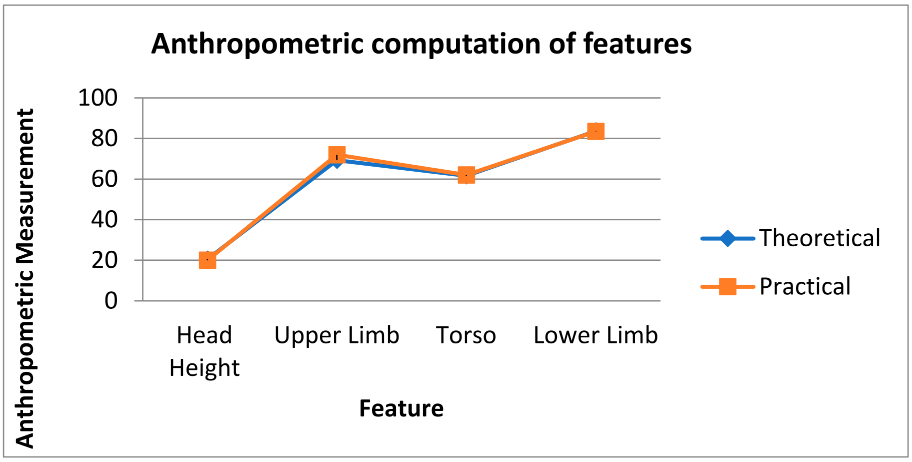

Figure 8. Analysis of anthropometric segments using theoretical and measured values.

Table 1. Comparison of theoretical and practical anthropometric values.

Feature	Theoretical (Ti)	Practical (Pi)	% Deviation (δi)
Head Height	20.5	20	−2.43%
Upper Limb	69.3	72	+3.90%
Torso	61.6	62	+0.65%
Lower Limb	83.7	83.5	−0.24%

The proposed anthropometric measurements are adapted from David [15] and evaluated for each subject using both theoretical estimates and actual height measurements. Equation (17) defines the deviation term (δ_i), which quantifies the difference between the theoretically computed values derived from anthropometric ratios and the corresponding measurements obtained through manual scaling. The deviation results show that the upper limb exhibits a maximum variation of 3.9% and a minimum deviation of 0.65%. These deviations collectively contribute to the overall accuracy, expressed as the Average Percentage Deviation (APD).

$$APD = \frac{Sum\ of\ all\ percentage\ deviations}{Number\ of\ features} \tag{18}$$

$$APD = \frac{\delta 1 + \delta 2 + \delta 3 + \delta 4}{4}$$

$$APD = \frac{2.43 + 3.90 + 0.65 + 0.24}{4} = 1.8\%$$

$$\text{Accuracy} = 100 - \text{APD} = 100 - 1.8\% = 98.2\%$$

Using the four selected features, the overall APD for one subject was obtained as 1.8%. Accordingly, the accuracy derived from the APD corresponds to 98.2%. These results demonstrate the effectiveness of the proposed anthropometric approach, yielding highly accurate posture estimation. The Average Percentage Deviation (APD) here quantifies the deviation between the estimated anthropometric measurements and the corresponding reference measurements.

Figure 9 presents the results for ten subjects using four anthropometric features: head height, torso height, upper limb length, and lower limb length. For each subject, both the theoretical (TH) feature computations and the practical (PR) measured values are recorded, as shown in Figure 9. The proposed method aligns closely with three of the feature lengths—head height, upper limb length, and lower limb length—showing minimal deviation between the TH and PR values. The torso measurements exhibit slightly higher differences, particularly for subjects 8, 9, and 10. This variation is attributed to the loose-fitting clothing worn by these subjects, which affected accurate torso estimation.

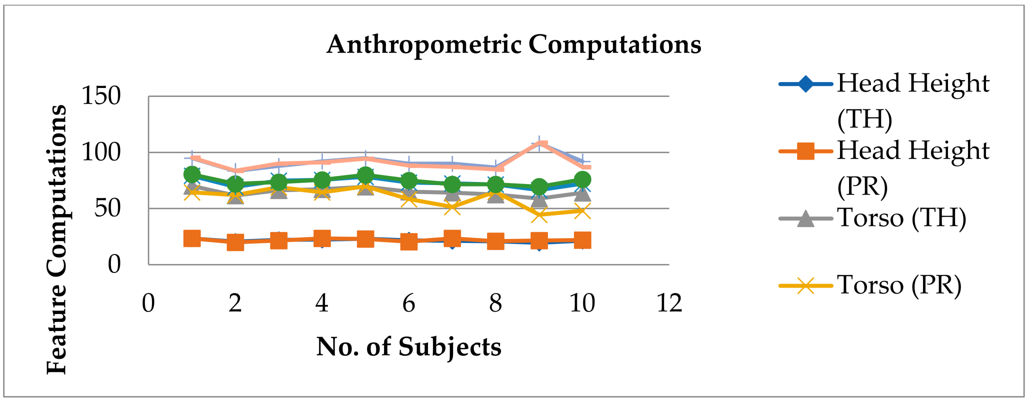

Figure 9. Subject-wise analysis of anthropometric feature variations.

Table 2 presents the APD and accuracy values computed using Expressions (17) and (18). The results summarize the anthropometric measurements of ten subjects across four features. The overall deviation between the theoretical (TH) and practical (PR) values for all four features across the ten subjects is 4.62%, corresponding to an accuracy of 95.4%. Accuracy values close to 95% were achieved for seven of the ten subjects, indicating consistently reliable performance. These outcomes confirm that the proposed photoanthropometric model analyzes posture highly effectively.

Table 2. Deviation and accuracy for 10 subjects.

Sub	Head (%)	Torso (%)	Upper Limb (%)	Lower Limb (%)	APD (%)	Accuracy (%)
S1	+0.43	−8.12	+1.64	+0.42	2.65	97.35
S2	−2.44	+0.65	+3.90	+0.24	1.81	98.19
S3	−2.71	+4.07	−1.74	+2.39	2.73	97.27
S4	+5.10	−3.85	−0.11	−0.91	2.49	97.51
S5	−0.61	+0.59	+2.17	−0.69	1.02	98.98
S6	−5.27	−9.92	+2.51	−1.96	4.91	95.09
S7	+10.33	−19.78	+3.65	−3.17	9.23	90.77
S8	+0.96	+4.17	+0.14	−1.97	1.81	98.19
S9	+9.53	−24.44	+4.61	+0.67	9.81	90.19
S10	+3.19	−24.95	+5.34	−5.52	9.75	90.25

The experimental evaluation of ten participants demonstrated a maximum individual posture estimation accuracy of 98.2%, while the proposed framework achieved an overall average recognition accuracy of 95.4%, demonstrating the effectiveness of the proposed photoanthropometric approach for real-time yoga pose analysis.

4.3. Experiment

Figure 10a–d presents the images analyzed using the proposed photoanthropometric method for evaluating yoga poses. A subject is shown performing the Tadasana sequence with standing and bending postures, with this being recorded using the vision-based setup. The upper row of images shows the neutral standing pose and the extended posture, whereas the lower row illustrates the left- and right-side bending positions. To perform Tadasana, the subject needs to stand in a straight position, as shown in Figure 10a. Moving to the next step, the subject needs to stretch their hands and then lift them upwards in line with their ears, as shown in Figure 10b. In the next step, the subject bends towards the left, making an angular movement reflecting Tiryak Tadasana, as shown in Figure 10c. The same posture is repeated towards the right, as depicted in Figure 10d. The captured images are processed using the developed LabVIEW 2019 software interface and are displayed on the laptop screen, where anthropometric features and posture deviations are computed in real time. This setup demonstrates the practical applicability of the system and confirms its ability to accurately extract body measurements during dynamic yoga poses. These experimental results are presented in the following YouTube link: https://youtube.com/shorts/b7gOHwQ2g1s. https://youtube.com/shorts/Rvp2Ds4m-VQ, accessed on 12 July 2026.

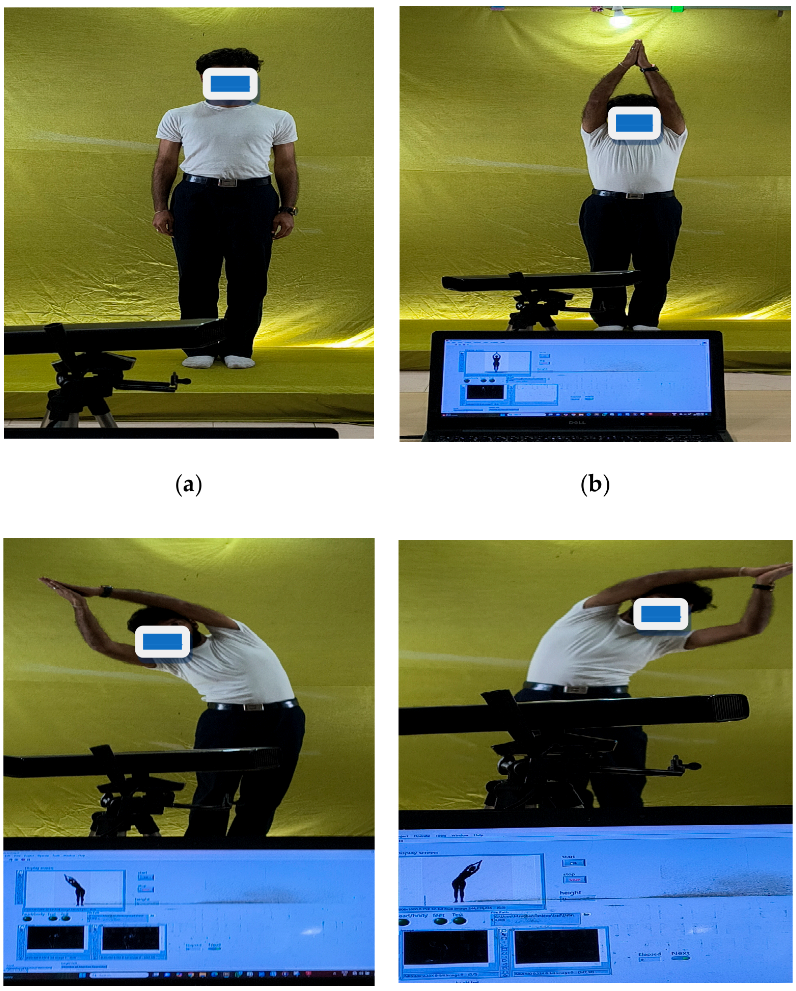

(**a**) (**b**)

(**c**) (**d**)

Figure 10. (**a**–**d**): Experimental evidence for photoanthropometric analysis of yoga poses.

Figure 11a–h demonstrate an experimental result in which the practitioner has been instructed to perform Tadasana and Tiryak Tadasana in such a way that the feet are kept together in the first experiment (Figure 11a–d) and then kept at a distance of 1.5 feet apart (Figure 11e–h). The experiment highlights the practitioner's flexibility, as it was observed that keeping the feet 1.5 feet apart and bending towards the right or left when performing Tiryak Tadasana was comfortable. The angular momentum here can be obtained as the maximum value without deviating from the asana.

(**a**) (**b**) (**c**) (**d**) (**e**) (**f**) (**g**) (**h**)

Figure 11. (**a**–**h**): Experimental evidence for photoanthropometric analysis of yoga poses with different foot spacing.

a. Standing straight to perform Tadasana with foot placed together.
b. Standing straight to perform Tadasana with foot placed together and hands stretched.
c. Standing straight to perform Tadasana with foot placed together and hands raised.
d. Bending right to perform Tiryak Tadasana with foot placed together.
e. Standing straight to perform Tadasana maintaining 1.5 feet distance between the foot.
f. Standing straight to perform Tadasana maintaining 1.5 feet distance between the foot and hands stretched.

g. Standing straight to perform Tadasana maintaining 1.5 feet distance between the foot and hands raised.

h. Bending right to perform Tiryak Tadasana maintaining 1.5 feet distance between the foot.

4.4. Comparison

Previous research [18] has demonstrated the detection of human yoga poses, such as Tadasana and Tiryak Tadasana, using a similar hardware setup. Figure 12a illustrates the captured edge representation of the human posture, which is further transformed into a skeleton model, as shown in Figure 12b. The generated skeleton models presenting the Tadasana and Tiryak Tadasana poses are presented in Figures 12c and 12d, respectively.

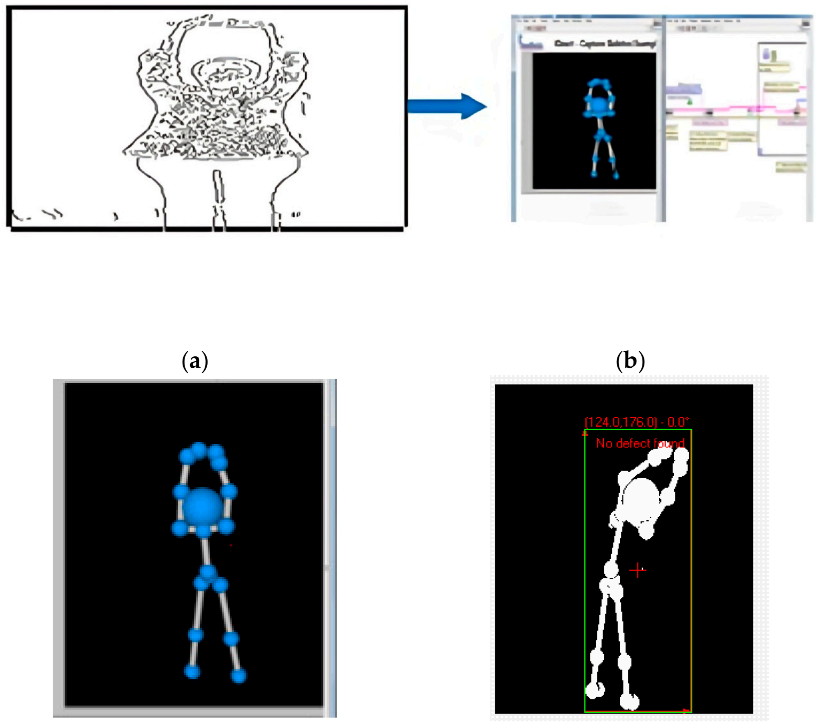

(**a**) (**b**) (**c**) (**d**)

Figure 12. (**a**–**d**): Identification and validation of skeleton during Tadasana and Tiryak Tadasana [18]. (**a**). Representation of Tadasana. (**b**). LabVIEW environment for the asana detection. (**c**). Front panel representation of Tadasana. (**d**). Bounding box representation of TiryakTadasana.

The proposed photoanthropometric framework has been compared with existing skeleton-based approaches as shown in Table 3. Previous research [18] on yoga pose analysis using skeletonization methods has achieved an accuracy of up to 89.67%. However, these approaches faced limitations in accurately validating upper limb wrist movements and lower limb foot positioning. In addressing these challenges, the proposed photoanthropometric framework demonstrates improved performance, achieving an accuracy of nearly 95.4%.

The proposed photoanthropometric approach using YOLO for yoga pose analysis has been described in the previous sections. This method is compared with other existing approaches used for sleep posture analysis and yoga pose recognition.

Although Table 4 provides a comparison between the proposed method and representative studies, the reported performance values should be interpreted with caution. It is shown that most prior studies have focused primarily on posture classification, with notable contributions from Mullerpatan et al. [19,20]. The compared methods were evaluated using different datasets, participant populations, hardware platforms, imaging conditions, and evaluation protocols. Consequently, a direct numerical comparison of accuracy may not fully reflect the relative performance of the individual approaches. Therefore, this comparison is intended to provide qualitative insight into the characteristics, advantages, and limitations of existing methods, while highlighting the novelty of integrating photoanthropometric analysis with YOLOv4-based human body localization for real-time yoga pose assessment. A comprehensive quantitative comparison using a common benchmark dataset and standardized evaluation protocol will be considered in future work.

Table 3. Comparative analysis of photoanthropometric and skeletonization approaches.

Comparison Metrics	Photoanthropometric	Skeletonization [18]
Neck-to-ankle identification	Accurate	Accurate
Wrist to finger tip	Accurate	Low
Foot length	Accurate	Low
Head movement	Accurate	Moderate
Computational cost	Fast	Requires more processing
Camera sensitivity	Depends on distance between practitioner and camera	Lower accuracy for limbs and torso

Table 4. Comparison of human posture identification approaches.

Reference	Posture Methods	Algorithms	Hardware	Pros	Accuracy	Cons
Wei et al. [7]	Skeleton-based method	HRNet, AGCN, MTCN, STSAM	Occlusion-free	Recognition accuracy of 93.83%		Camera alignments
Raza et al. [9]	Random Forest method	K-fold approach, Hyper parameter tuning	Remote monitoring and guidance capability	High performance score	0.998	Cannot be used for real-time identification
N. Dalal et al. [8]	HoG Descriptors	Gradient Computations, Linear SVM	Reducing false positives	89% at 10-4 FPPW		Parts-based model is not available
Mullerpatan et al. [19,20]	Kinematics of Suryanamaskar	Plug-in Gait	3D motion capture, CPU	Postural balance kinematics analysis	Not defined	More hardware used
Sravanthi et al. [21,22]	Sleep Posture	Random Forest, ML	Ultrasonic, FPGA	Low computation time	>96%	Used at a certain level
Proposed	Tadasana yoga pose	Anthropometric and YOLO bounding box	LabVIEW, Kinect Xbox 360, CPU	Inference level yoga pose analysis	95.4%	Twisted yoga pose analysis

5. Conclusions

In this work, a unified photoanthropometric framework is presented for real-time yoga pose analysis by integrating calibrated bounding box extraction and AI-based classification. The system employed YOLOv4 for posture localization and utilized LabVIEW Vision IMAQ together with LabVIEW ML to construct a complete end-to-end processing pipeline. A ten-subject experimental study was conducted to assess the reliability of the extracted anthropometric features. The overall accuracy achieved across subjects was 95.4%, with the best individual subject accuracy reaching 98.2%. The photoanthropometric process demonstrated effective performance through the combined use of anthropometric modeling and YOLO-based detection. Overall, the proposed system provides a robust and scalable foundation for advancing automated yoga pose analysis and embedded wellness technologies. In the future, this framework can be extended to include twisted and complex yoga poses.

Author Contributions: Conceptualization: T.P.K.N. and S.S.R.; methodology: T.P.K.N. and S.S.R.; validation: T.P.K.N. and S.S.R.; writing—original draft preparation, T.P.K.N. and S.S.R.; writing—review and editing, T.P.K.N. and S.S.R. All authors have read and agreed to the published version of the manuscript.

Funding: This research received no external funding.

Data Availability Statement: The original contributions presented in this study are included in the article. Further inquiries can be directed to the corresponding author.

Acknowledgments: The LabVIEW Tool and studio environment were provided by the B V Raju Institute of Technology, Medak (Dist.), Narsapur. M C Chinnaiah, Dept. of ECE, BVRIT for providing access to the Lab tools and the environment.

Conflicts of Interest: The authors declare no conflicts of interest.

References

1. Available online: https://www.who.int/southeastasia/news/opinion-editorials/detail/yoga-for-humanity (accessed on 25 March 2026).
2. Rajendran, A.K.; Sethuraman, S.C. A Survey on Yogic Posture Recognition. *IEEE Access* **2023**, *11*, 11183–11223. [CrossRef]
3. Satyanarayanan, M. Pervasive computing: Vision and challenges. *IEEE Pers. Commun.* **2001**, *8*, 10–17. [CrossRef]
4. Gallego, G.; Delbruck, T.; Orchard, G.M.; Bartolozzi, C.; Taba, B.; Censi, A.; Leutenegger, S.; Davison, A.J.; Conradt, J.; Daniilidis, K.; et al. Event-Based Vision: A Survey. *IEEE Trans. Pattern Anal. Mach. Intell.* **2022**, *44*, 154–180. [CrossRef] [PubMed]
5. Hewett, T.E.; Myer, G.D.; Ford, K.R.; Heidt, R.S., Jr.; Colosimo, A.J.; McLean, S.G.; Van den Bogert, A.J.; Paterno, M.V.; Succop, P. Biomechanical measures of neuromuscular control and valgus loading of the knee predict anterior cruciate ligament injury risk in female athletes: A prospective study. *Am. J. Sports Med.* **2005**, *33*, 492–501. [CrossRef] [PubMed]
6. Zhang, S.; Wei, Z.; Nie, J.; Huang, L.; Wang, S.; Li, Z. A review on human activity recognition using vision-based method. *J. Healthc. Eng.* **2017**, *2017*, 3090343. [CrossRef] [PubMed]
7. Wei, G.; Zhou, H.; Zhang, L.; Wang, J. Spatial–Temporal Self-Attention Enhanced Graph Convolutional Networks for Fitness Yoga Action Recognition. *Sensors* **2023**, *23*, 4741. [CrossRef] [PubMed]
8. Dalal, N.; Triggs, B. Histograms of Oriented Gradients for Human Detection. In *Proceedings of the IEEE Computer Society Conference on Computer Vision and Pattern Recognition (CVPR)*; IEEE: New York, NY, USA, 2005; pp. 886–893.
9. Raza, A.; Qadri, A.M.; Akhtar, I.; Samee, N.A.; Alabdulhafith, M. LogRF: An Approach to Human Pose Estimation Using Skeleton Landmarks for Physiotherapy Fitness Exercise Correction. *IEEE Access* **2023**, *11*, 107930–107939. [CrossRef]
10. Li, Y.; Yang, C.; Zhang, L.; Xia, R.; Fan, L.; Xie, W. A Novel SURF Based on a Unified Model of Appearance and Motion-Variation. *IEEE Access* **2018**, *6*, 31065–31076. [CrossRef]
11. Bhandage, V.; Prabhu, S.; Hadimani, B.S.; Chadaga, K.; Sampathila, N.; Shetty, S. Classification of Surya Namaskar Yoga Asanas: A Sequential Combination of Predominant Poses for Physical and Mental Health. *IEEE Access* **2024**, *12*, 102027–102034. [CrossRef]
12. *IEEE Standard 978-1-5044-3780 6*; IEEE Industry Connections (IEEE-IC) 3D Body Processing (3DBP) 1221 Initiative—An Introduction. IEEE: New York, NY, USA, 2017.
13. Sarafianos, N.; Nikou, C.; Kakadiaris, I.A. Predicting privileged information for height estimation. In *Proceedings of the 2016 23rd International Conference on Pattern Recognition (ICPR), Cancun, Mexico, 4–8 December 2016*; IEEE: New York, NY, USA, 2016; pp. 3115–3120. [CrossRef]
14. Kaashki, N.N.; Hu, P.; Munteanu, A. Deep Learning-Based Automated Extraction of Anthropometric Measurements From a Single 3-D Scan. *IEEE Trans. Instrum. Meas.* **2021**, *70*, 5015414. [CrossRef]
15. Winter, D.A. *Biomechanics and Motor Control of Human Movement*; John Wiley & Sons: Hoboken, NJ, USA, 2009.
16. Mathis, A.; Mamidanna, P.; Cury, K.M.; Abe, T.; Murthy, V.N.; Mathis, M.W.; Bethge, M. DeepLabCut: Markerless pose estimation of user-defined body parts with deep learning. *Nat. Neurosci.* **2018**, *21*, 1281–1289. [CrossRef] [PubMed]
17. Colyer, S.L.; Evans, M.; Cosker, D.P.; Salo, A.I. A review of the evolution of vision-based motion analysis and the integration of advanced computer vision methods towards developing a markerless system. *Sports Med.-Open* **2018**, *4*, 24. [CrossRef] [PubMed]
18. Chinnaiah, M.C.; Nandan, T.P.K.; Haritha, P.; Dubey, S.; Pasha, I.A. A New Deliberation of Embedded based Assistive System for Yoga. In *Proceedings of the 2018 8th International Symposium on Embedded Computing and System Design (ISED), Cochin, India, 13–15 December 2018*; IEEE: New York, NY, USA, 2018; pp. 42–47. [CrossRef]
19. Mullerpatan, R.P.; Agarwal, B.M.; Shetty, T.; Nehete, G.R.; Narasipura, O.S. Kinematics of suryanamaskar using three-dimensional motion capture. *Int. J. Yoga* **2019**, *12*, 124–131. [CrossRef] [PubMed]
20. Mullerpatan, R.P.; Agarwal, B.M.; Shetty, T.V. Exploration of muscle activity using surface electromyography while performing surya namaskar. *Int. J. Yoga* **2020**, *13*, 137–143. [CrossRef] [PubMed]

21. Sravanthi, M.; Gunturi, S.K.; Chinnaiah, M.C.; Vani, G.D.; Basha, M.; Janardhan, N.; Krishna, D.H.; Dubey, S. Hardware-Accelerated Non-Contact System for Sleep Disorder Monitoring and Analysis. *Sensors* **2025**, *25*, 2747. [CrossRef] [PubMed]
22. Sravanthi, M.; Gunturi, S.K.; Chinnaiah, M.C.; Lam, S.-K.; Vani, G.D.; Basha, M.; Janardhan, N.; Krishna, D.H.; Dubey, S. A Field-Programmable Gate Array-Based Adaptive Sleep Posture Analysis Accelerator for Real-Time Monitoring. *Sensors* **2024**, *24*, 7104. [CrossRef] [PubMed]